BL28XU
RISING II

1. Introduction

BL28XU mainly develops technology for *in situ* observations of the reaction inside storage batteries via the energy-dispersive confocal diffraction technique, X-ray diffraction spectroscopy analysis, hard X-ray photoelectron spectroscopy, and so forth. The RISING2 project had been running from FY2016 to FY2020 as a contract research project of the New Energy and Industrial Technology Development Organization (NEDO) to promote technology development for the practical uses of storage batteries. On the basis of the results of RISING, the predecessor of RISING2, specific research focuses on three subjects for storage batteries on a wide spatiotemporal scale: (1) the elucidation of reaction distribution generation factors, (2) the analysis of active material reactions and nonequilibrium behaviors, and (3) the elucidation of electrode/electrolyte interface phenomena. In addition, the technologies to address the following subjects have been developed in the RISING2 project: (4) the elucidation of the formation mechanism of random materials, such as electrolytic solution and electrolytes at the electrode interface, and (5) the elucidation of thermodynamic or physical instability phenomena inside the storage batteries. The RISING3 project, the successor of RISING2 launched in FY2021, is ongoing to focus on these subjects by developing technologies with sufficient spatial and time resolutions. Hereinafter, we introduce representative achievements in FY2020.

2. Operando XAFS of manganese oxide ORR catalysts in concentrated alkaline media

Rechargeable zinc-air batteries (ZAB) have a theoretical energy density of 1300 Wh kg^{-1} [1], which is several times higher than that of Li rechargeable batteries, making them particularly attractive candidates for next-generation energy storage applications. For realizing highly efficient energy storage in ZAB, a critical issue is to reduce the overpotentials of four-electron ($4e^-$) transfer oxygen reduction reaction (ORR). In recent years, $La_{0.7}Sr_{0.3}Mn_{0.9}Ni_{0.1}O_{3-\delta}$ (LSMN) has been found to solely facilitate the four-electron transfer ORR in 4 M KOH without cocatalysts of carbon and precious metals [2]. Herein, we demonstrated that the $4e^-$ transfer pathway is triggered by the formation of the surface oxygen vacancy on LSMN by means of *operando* X-ray absorption spectroscopy (XAS) with epitaxial thin film electrodes under strongly alkaline conditions.

Operando Mn *K*-edge XAS analysis was carried out on a Spring-8 BL28XU undulator beamline by recording the *Kα* X-ray fluorescence. The LSMN thin film (20 nm thickness) was deposited on an NSTO wafer (10 mm × 10 mm), and a thin Au lead wire (0.05 mmϕ) was attached to the back side of the wafer with a small amount of Ag paste. The samples thus prepared were used for the *operando* measurements.

The concentrated alkaline solution showed a relatively high absorbance for the X-ray. At the Mn *K*-edge (6,550 eV), the X-ray intensity is roughly attenuated to 1/e after passing through a 260-μm-thick 4 M KOH layer. Thus, the *operando* XAS analysis probed the surface of the LSMN working

electrode covered with a thin layer of the KOH solution. To this end, the NSTO wafer with a 20-nm-thick LSMN film was placed vertically in the spectroelectrochemical cell, and a Teflon nozzle was contacted with the upper side of the wafer (Figs. 1(a)–1(c)). The electrolyte flowed out of the nozzle and down the hydrophilic film surface, covering the entire surface of the working electrode as a submillimeter-thick fluid layer, as confirmed with a magnifying glass (Fig. 1(d)). The synchrotron X-ray microbeam was irradiated on the film surface at an oblique angle of about 0.3°, which is less than the critical angle of total reflectance at the water/solid interface. The fluorescence yields were corrected with the silicon drift detector (SDD). The details of the operando XAS are described elsewhere [3].

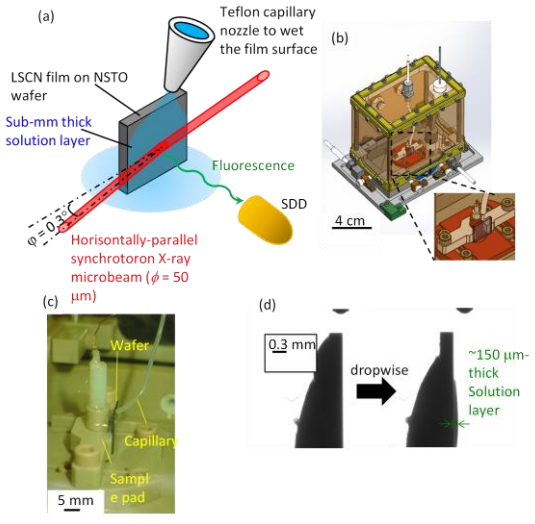

Fig. 1. Concepts of operando XAS under ORR. (a) Methodology for probing the surface of the LSMN electrode during ORR. The electrolyte droplet from the nozzle at the upper end of the wafer wets the whole surface with a sub-millimeter-thick liquid layer. The synchrotron X-ray probes the surface under the liquid layer. (b) Schematic view of the optoelectrochemical cell used for XAS. (c) Magnified image of the sample mounted in the cell with an attached capillary nozzle. (d) Magnified image of a liquid layer formed on the film surface by dripping the KOH solution.

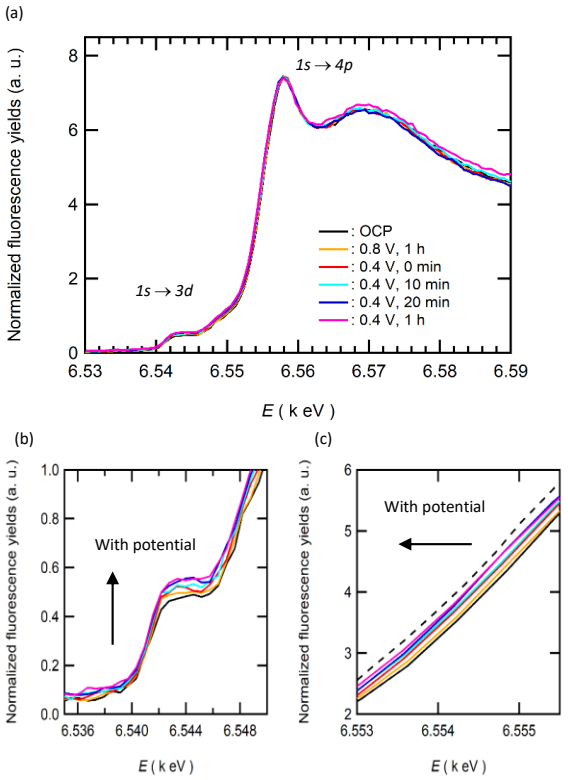

Fig. 2. *Operando* Mn *K*-edge XANES of the (100) LSMN film for ORR in an O_2-saturated 4 M KOH solution at the OCP (~0.3 V vs RHE) and at 0.8 and 0.4 V vs RHE. (a) XANES spectra and expanded (b) pre-edge and (c) adsorption edge regions. The time in (a), (c), and (d) represents the duration for which each potential was maintained.

Figure 2 shows the X-ray absorption near edge spectroscopy (XANES) data at the Mn *K*-edge for the LSMN films undergoing ORR

potentiostatically at the open circuit potential (OCP) and at 0.4 and 0.8 V vs RHE in 4 M KOH. In *operando* XAS, the LSMN yielded a very small *i* at 0.8 V vs RHE, whereas it exhibited remarkable activation during ORR at 0.4 V vs RHE with *i* increasing three times after 1 h. The Mn *K*-edge XANES yielded a vertically rising main edge with a maximum peak at approximately 6550 eV and a pre-edge peak at approximately 6540 eV (Fig. 2(a)). The pre-edge intensity increased considerably with the cathodic polarization level (Fig. 2(b)), which proved that oxygen vacancies were incorporated into the LSMN surface with the progress of ORR in concentrated alkaline media because the pre-edge features are very sensitive to a change from a centrosymmetric to a non-centrosymmetric coordination environment of Mn atoms by oxygen vacancy creation.

3. Synchronized operando analysis of graphite negative electrode of Li ion battery

The first preparation of the Li-graphite intercalation compound (Li-GIC) was attempted by Hérold in 1955 [4]. Since then, many studies have been conducted and reported mainly by research groups in France, and with regard to the stage I and II compounds, it is clarified that they have the p(√3×√3)R30°-type in-plane structure as shown in Fig. 3 [5,6].

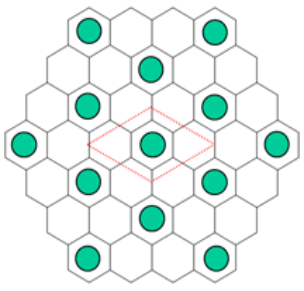

Fig. 3. p(√3×√3)R30°-type in-plane structure.

Although there have been many reports since the 1970s, no detailed discussion has been done so far on the intercalation mechanism and in-plane structure of higher stage compounds. The first reason is that the concentration of Li species decreases in the higher stages. The second reason is the strong preferred orientation of graphite. Such reasons make it difficult to clarify the intercalation mechanism and in-plane structure. To improve the performance of the Li-ion battery, it is essential to investigate the detailed structure change of the graphite electrode during the charge/discharge process. To elucidate the intercalation mechanism and structure change not only along the *c*-axis but also along the *a*,*b*-axes, we traced the intercalation reaction in the Li-ion battery negative electrode by synchrotron radiation diffraction.

The Al-laminated half-cell composed of natural graphite and Li electrodes (20 × 20 mm) in 1M-$LiPF_6$/EC+EMC(3:7) was assembled. Then, it was once charged and discharged before the operando measurement. After that, the synchrotron radiation measurement was carried out during the second cycle in the range of 0.05–2.5 V at 0.1 C with the BL28XU beamline. A high-energy X-ray with a beam size of 0.5 × 0.2 mm and a wavelength of 0.049592 nm was used to obtain 2D diffraction patterns in the transmission geometry. The diffraction data were detected with a PILATUS 100K 2D detector (Rigaku Corporation). The exposure time was set to 10 s, and about 7200 diffraction profiles were obtained during the charge and discharge processes. To analyze the dataset thus obtained in conjunction with the charge/discharge curves and their differential curves (V-dQ/dV), an analysis software program called “Profile Chaser” was newly developed. By using this software

program, all the 00*l* and *hk*0 diffractions during the charge and discharge processes are loaded automatically in the computer. The profiles were continuously displayed on a monitor as a series of diffraction profiles in conjunction with the compositions estimated from the charge/discharge curves, so that the profile change was traced from the monitor as shown in Fig. 4.

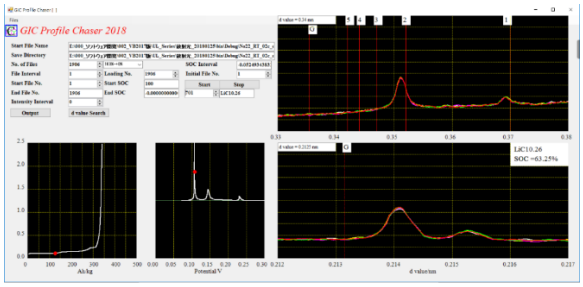

Fig. 4. Analysis window of profile chaser.

Figure 5 shows the profile changes of two-dimensional 100 and 002 diffractions of graphite in the intercalation process with the interval of 1% SOC. As can be seen, the structure change appeared not only in the 002 profile but also in the 100 profile, and the behavior of the profile change along the c-axis seems to be linked with that of the in-plane structure change along the *a*,*b*-axes.

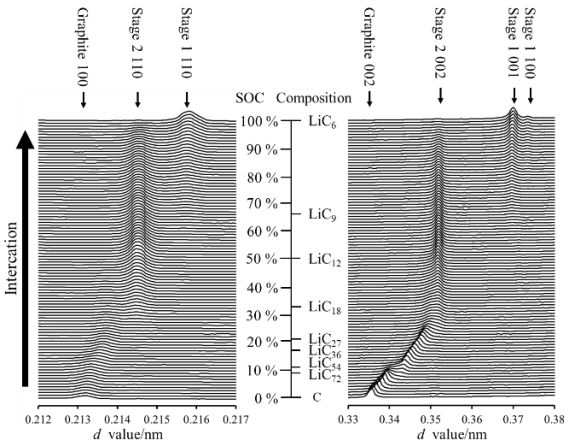

Fig. 5. Changes in 100 and 002 SRD profiles of graphite in the intercalation process.

Acknowledgements

This work is based on the results obtained from a project, "Research and Development Initiative for Scientific Innovation of New Generation Batteries (RISING2)", JPNP16001, commissioned by the New Energy and Industrial Technology Development Organization (NEDO).

Yoshitaka Aoki[*1], Yuki Sato[*2], Sho Kitano[*1], Hiroki Habazaki[*1], Hiroyuki Fujimoto[*3], and So Fujinami[*3]

[*1] Faculty of Engineering, Hokkaido University

[*2] Graduate School of Chemical Sciences and Engineering, Hokkaido University

[*3] Office of Society–Academia Collaboration for Innovation, Kyoto University

References:

[1] Li, Y. & Dai, H. (2014). *Chem. Soc. Rev.* **43**, 5257–5275.

[2] Aoki, Y. Tsuji, E. Motohashi, T. Kowalski, D. & Habazaki, H. (2018). *J. Phys. Chem. C* **122**, 22301–22308.

[3] Aoki, Y. Takasse, K. Kiuchi, H. Kowalski, D. Sato, Y. Kitano, S. & Habazaki, H. (2021). *J. Am. Chem. Soc.* **143**, 6505–6515.

[4] Hérold, A. (1955). *Bull. Soc. Chim. France* **187**, 999.

[5] Guerard, D. & Hérold, A. (1975). *Carbon* **13**, 337.

[6] Dresselhaus, M. S. & Dresselhaus, G. (1981). *Adv. Phys.* **30**, 139.